Journal of Materials Chemistry B

ROYAL SOCIETY OF CHEMISTRY

PAPER

View Article Online
View Journal | View Issue



Cite this: J. Mater. Chem. B, 2023, 11, 5460

# Amikacin@$SiO_2$ core@shell nanocarriers to treat pulmonal bacterial infections

Mark Rutschmann,[a] Natalja Redinger,[bc] Ulrich E. Schaible[*bcd] and Claus Feldmann[*a]

Received 30th November 2022,
Accepted 28th April 2023

DOI: 10.1039/d2tb02609k

rsc.li/materials-b

AMC@$SiO_2$ core@shell nanocarriers (AMC: amikacin) are realized and contain an exceptionally high drug load of 0.8 mg $mg^{-1}$ (*i.e.* 80% AMC of total nanocarrier mass). They are prepared *via* a solvent–antisolvent approach with AMC nanoparticles formed in a first step, which are then covered and stabilised by a thin silica shell in a one-pot synthesis. In total, the core@shell nanocarriers exhibit a mean diameter of 240 nm with an inner AMC core of 200 nm and an outer silica shell of 20 nm. Subsequent to synthesis, the nanocarriers can be stored in frozen dimethylsulfoxide (DMSO) and applied directly after warming to room temperature with particle contents of 5 mg $mL^{-1}$. Size, structure, and composition of the AMC@$SiO_2$ core@shell nanocarriers are evidenced by electron microscopy (SEM, TEM), spectroscopic methods (EDXS, FT-IR, UV-Vis), as well as X-ray powder diffraction and elemental analysis. As proof-of-concept, the AMC release and the activity of the novel nanocarriers are tested against two relevant, difficult-to-treat and notoriously multidrug resistant, bacterial pathogens: *Mycobacterium tuberculosis* (*M.tb.*) and *Mycobacterium abscessus* (*M.abs.*). Colloidal stability, storage stability, high drug load, and activity of the AMC@$SiO_2$ core@shell nanocarriers are promising for, *e.g.*, aerosol-type pulmonal application.

**10th Anniversary Statement**

The *Journal of Materials Chemistry* offers the unique option to present and to introduce new materials with specific material properties with a wide scope of disciplines ranging from chemistry, physics, and biology to medicine. For about 10 years, we have predominately contributed to JMC-C. Due to our recent activities on nanocarriers for multimodal imaging and drug delivery, JMC-B is now becoming another first-choice journal for us to bridge the gap between new materials and fundamental chemistry with an evaluation of these materials in regard to biomedical application.



## Introduction

The aminoglycoside antibiotic amikacin (AMC) is applied to treat acute severe bacterial infections, usually caused by Gram-negative bacterial and mycobacterial pathogens such as *Pseudomonas*, *Klebsiella*, or *Enterobacter*.[1] Its antimicrobial activity is based on interfering with protein synthesis by binding to bacterial ribosomes. AMC is widely used in patients with bacterial pneumonia, intra-abdominal infections, meningitis, sepsis, and urinary-tract infections.[1] Moreover, in the case of failed first-line anti-tuberculosis therapy, AMC is employed as a second-line agent to multidrug-resistant (MDR) *M. tuberculosis* infections in combination with additional antibiotics.[1,2]

Upon long-term treatment, AMC is known to be oto- and nephrotoxic and may cause hearing loss and kidney damage as severe adverse effects.[1,3] Since there is no resorption from intestine, the antibiotic needs to be injected intravenously (*i.v.*) or intramuscular. Systemic application promotes the aforementioned adverse effects. In order to overcome systemic effects, encapsulation of AMC in suitable nanocarrier systems is an intriguing alternative.[1] In comparison to other drugs, and especially in comparison to chemotherapeutic agents,[4] nanocarriers-based approaches were rarely reported for AMC, in general. Among these approaches, AMC was most often encapsulated in different types of polymers and biopolymers,[1a,5] including poly(lactic-*co*-glycolic acid) (PLGA), chitosan, or RNA.[6] Hereof, PGLA-based nanocarriers turned out to be most promising due to currently the highest AMC loads of 10–40 μg $mg^{-1}$.[6a–d] Moreover, AMC was formulated as liposome-based suspension with AMC loads of 0.5%.[7] In addition to polymer matrices and

[a] *Institute of Inorganic Chemistry, Karlsruhe Institute of Technology (KIT), Engesserstraße 15, 76131 Karlsruhe, Germany. E-mail: claus.feldmann@kit.edu*
[b] *Research Center Borstel, Leibniz Lung Center, Priority Area Infections, Division Cellular Microbiology, Parkallee 1-40, 23845 Borstel, Germany*
[c] *German Center for Infection Research (DZIF), Site Hamburg-Lübeck-Borstel-Riems, 23845 Borstel, Germany. E-mail: uschaible@fz-borstel.de*
[d] *University of Luebeck, 23562 Luebeck, Germany*

liposomes, further concepts describe AMC adhered on silver and gold nanoparticles,[8] as well as graphene aerogels.[9] As current limitations, these nanoparticle-based approaches only allow comparably low AMC loads ($\leq$40 μg mg$^{-1}$ or $\leq$4% of total nanoparticle mass) with large particle sizes (200 nm up to several micrometers). Beside polymer-derived nanocarriers, silica and specifically mesoporous silica nanoparticles were widely applied for drug delivery,[10] also including anti-tuberculosis drugs.[11] Although widely applied for drug delivery, surprisingly and to the best of our knowledge, silica-based nanocarriers were not described for the transport and release of AMC.

In the following, we show the synthesis and characterisation of AMC@$SiO_2$ core@shell nanocarriers with an exceptional AMC load of 0.8 mg mg$^{-1}$ or 80% of the total nanocarrier mass for the first time. This drug load belongs to the highest drug loading of silica nanoparticles at all. The activity of the AMC@$SiO_2$ core@shell nanocarriers was tested against *Mycobacterium tuberculosis* (*M.tb.*) and *Mycobacterium abscessus* (*M.abs.*) as representatives of important multidrug-resistant and facultative intracellular pathogens causing either tuberculosis or non-tuberculous mycobacterial (NTM) infections in immunocompromised patients such as those with cystic fibrosis or ventilator-associated pneumonia.[12]

## Results and discussion

### Synthesis of AMC@$SiO_2$ nanocarriers

The general challenge in regard of the synthesis of AMC@$SiO_2$ core@shell nanocarriers relates to the need to encapsulate a highly polar hydrophilic drug (amikacin) into a highly polar hydrophilic shell (silica). A typical way for this is a microemulsion approach[13] with the hydrophilic drug dissolved in the aqueous droplet phase, followed by a controlled hydrolysis of a suitable silica precursor (*e.g.* tetraethylorthosilicate, TEOS), which is added to the non-polar dispersant phase of the microemulsion system.[13,14] Although widely applied, such microemulsion-based approach has certain restrictions such as the low amount of nanocarriers that can be obtained per volume of the microemulsion (*e.g.* 5–10 mg per 50 mL) or the low drug load in the limited volume of the aqueous droplet (*e.g.* 1–5 mL of water per 50 mL of microemulsion). To solve this problem, we here apply a modified solvent–antisolvent approach. In principle, such strategy is well-known to prepare micron-sized drug nanoparticles, but it is typically applied for lipophilic drugs being insoluble in water.[15] The realisation of hydrophilic AMC nanoparticles *via* a solvent–antisolvent approach is here shown for the first time (Fig. 1).

To obtain AMC@$SiO_2$ core@shell nanocarriers *via* a solvent–antisolvent approach, first of all, a saturated solution of AMC in water as the ''solvent'' was prepared (Fig. 1b). As a highly polar drug, AMC is well soluble in water (80 mg in 0.7 mL $H_2O$). This solution was injected into a larger volume of ethanol (50 mL), serving as the ''antisolvent'', with vigorous stirring at 70 °C. In contrast to water, AMC is more-or-less insoluble in ethanol, so

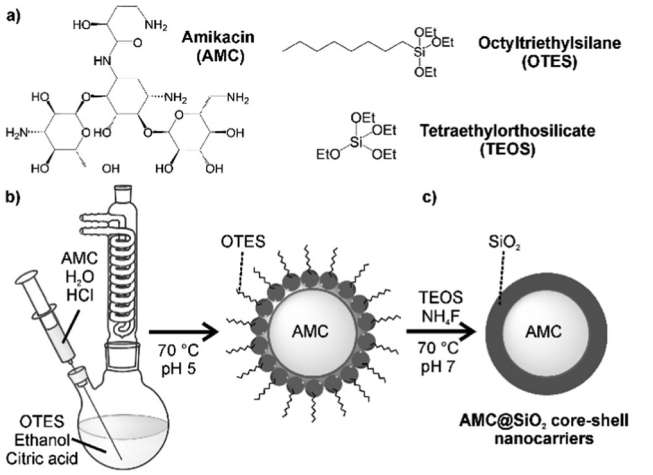


Fig. 1 Schematic illustration of the synthesis of AMC@$SiO_2$ core@shell nanocarriers: (a) starting materials, (b) nucleation *via* a solvent–antisolvent approach, (c) densification and thickening of silica shell.

that – in accordance with the La Mer–Dinegar model – nanoparticles are formed.[16] Thereby, a fast addition and a slightly elevated temperature support the nucleation process. The as-formed AMC nanoparticles, however, are colloidally not stable in ethanol and show agglomeration and precipitation on a time-scale of about 10 minutes. To stabilise the AMC nanoparticles, a low amount of octyltriethoxysilane (OTES) (30 μL) was added to the ethanol suspension, which, moreover, was slightly acidified (0.1 mL 0.1 M HCl) (Fig. 1b). Acidification catalyses the hydrolisation of the ethoxysilane groups of OTES to highly polar silanol (Si–OH) groups,[17] which coordinate to the surface of the as-formed polar AMC nanoparticles, whereas the less-polar octylsilane groups of OTES are directed to the ethanol phase. Acidic conditions as well as low quantities of fluoride, after addition of $NH_4F$, promote a cross-linking of the silanol groups at the AMC particle surface (Fig. 1c).[18]

To increase the thickness of the as-formed thin silica layer on the AMC nanoparticles, TEOS was added (Fig. 1c). In order to promote a growth of the already established silica shell over the nucleation of novel $SiO_2$ nanoparticles, TEOS was slowly added. Moreover, hydrolysis and cross-linking of the silanol groups were again supported by acidic conditions and addition of $NH_4F$. Subsequent to the synthesis, the as-prepared colourless AMC@$SiO_2$ core@shell nanocarriers were purified by centrifugation/redispersion from/in ethanol to remove remaining starting materials and salts. Finally, the AMC@$SiO_2$ core@shell nanocarriers can be dried in vacuum at room temperature to obtain powder samples, or they were redispersed in ethanol or dimethylsulfoxide (DMSO) with 5 mg mL$^{-1}$ of the nanocarriers. These suspensions are colloidally stable over several months. In particular, DMSO is useful as this solvent is also approved for clinical application (even intravenously).[19]

### Characterisation of AMC@$SiO_2$ nanocarriers

First of all, size, size distribution, and nanostructure of the as prepared AMC@$SiO_2$ nanocarriers were examined. To this

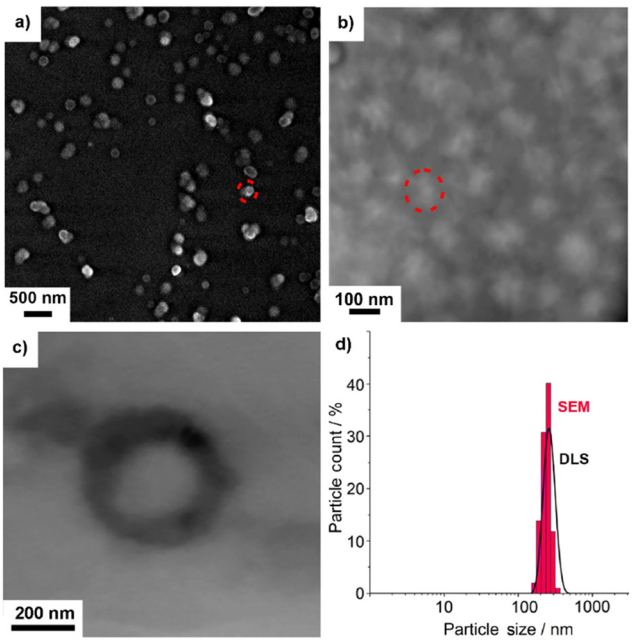


Fig. 2 Size and structure of the as-prepared AMC@$SiO_2$ core@shell nanocarriers: (a and b) SEM overview images at different levels of magnification with selected nanocarriers indicated by red dots, (c) STEM detail image, (d) size distribution according to SEM and DLS.

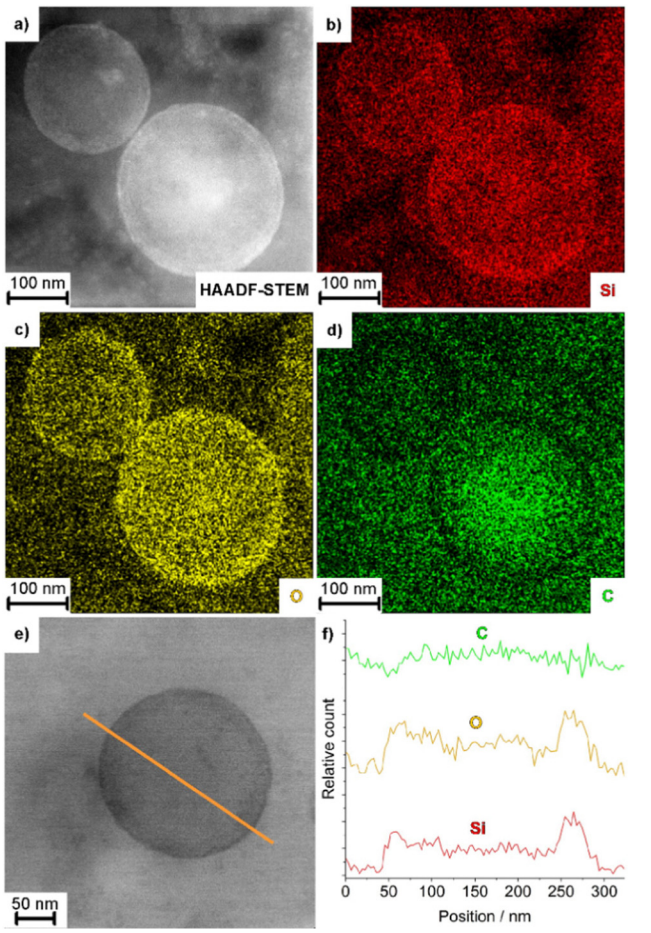


Fig. 3 Nanostructure of AMC@$SiO_2$ core@shell nanocarriers: (a) HAADF-TEM image, (b–d) EDXS area scans (Si–K, O–K, C–K lines used for analysis) of the nanostructure shown in (a), (e and f) EDXS line scan with (f) element mapping along the orange line in (e).

concern, dynamic light scattering (DLS) and electron microscopy were used. DLS analysis of suspensions in ethanol and DMSO exhibit mean hydrodynamic diameters of 253 ± 41 nm (ethanol) and 233 ± 39 nm (DMSO) with narrow size distribution (Fig. 2d). Scanning electron microscopy (SEM) shows a spherical shape of the nanocarriers with a particle diameter of 234 ± 39 nm (Fig. 2a, b and d), which is in accordance with the larger hydrodynamic diameter stemming from DLS analyses (Fig. 2d). This mean size was calculated by statistical evaluation of 150 nanoparticles on SEM images. Scanning transmission electron microscopy (STEM) elucidates the structure of the nanocarriers with an inner cavity about 200 nm in size and an outer wall, about 20 nm in diameter (Fig. 2c).

To prove the presence of the core@shell-type nanostructure and composition, transmission electron microscopy (TEM) and energy-dispersive X-ray spectroscopy (EDXS) were conducted. High-angle annular dark-field (HAADF)-TEM, first of all, confirms the presence of an inner cavity and an outer $SiO_2$ shell (Fig. 3a and e). EDXS areas scans show element mappings of Si, C, and O (Fig. 3b–d). Here, the higher concentration of Si and O in the outer shell (compared to the inner cavity) and the higher concentration of C in the inner cavity (compared to the outer shell) are indicative. Furthermore, an EDXS line scan also confirms the nanostructure of the AMC@$SiO_2$ core@shell nanocarriers with an inner cavity diameter of 170–220 nm and a shell thickness of 30–50 nm (Fig. 3e) and an element distribution similar to the EDXS area scans with a carbon-rich cavity and a silica-rich shell (Fig. 3f).

Beside size and nanostructure of the AMC@$SiO_2$ core@shell nanocarriers, their chemical composition was examined. To this regard, Fourier-transformed infrared (FT-IR) spectroscopy shows vibrations of $SiO_2$ ($\nu$(Si–O–Si): 1250–950, $\nu$(Si–OH): 950–880, $\delta$(Si–O–Si): 825–650 $cm^{-1}$), remaining octyl groups ($\nu$(C–H): 3000–2835 $cm^{-1}$), and AMC ($\nu$(O–H): 3500–3000, $\nu$(N–H): 3400–3000, $\nu$(C–H): 3000–2835, $\delta$(N–H): 1690–1520, $\delta(CH_3/CH_2)$: 1465–1438, $\delta$ $CH_3$): 1395, $\nu$(C–O): 1130–1000 $cm^{-1}$) (Fig. 4a). Furthermore, X-ray powder diffraction (XRD) indicates the nanocarriers to be non-crystalline, which is to be expected in regard of the low temperature of synthesis (Fig. 4b). Such non-crystalline drug reservoir was also reported to be advanta-geous in regard of a continuous release and fast distribution in comparison to crystalline drug particles.[15a]

Total thermal combustion *via* thermogravimetry (TG) shows a two-step decomposition (Fig. 4c). Thereof, the first step at 50–100 °C (10.2 wt%) can be ascribed to residual ethanol adhered to the particle surface. The second decomposition (150–600 °C, 81.0 wt%) can be related to the decomposition of all organic components in the AMC@$SiO_2$ nanocarriers. The solid residue (8.8 wt%) represents $SiO_2$. In addition to TG, elemental analysis (EA) results in C/H/N contents of 35/4.8/7.8 wt%. As only AMC contains nitrogen, 7.8 wt% N, 4.6 wt% H, and 30 wt% C

 

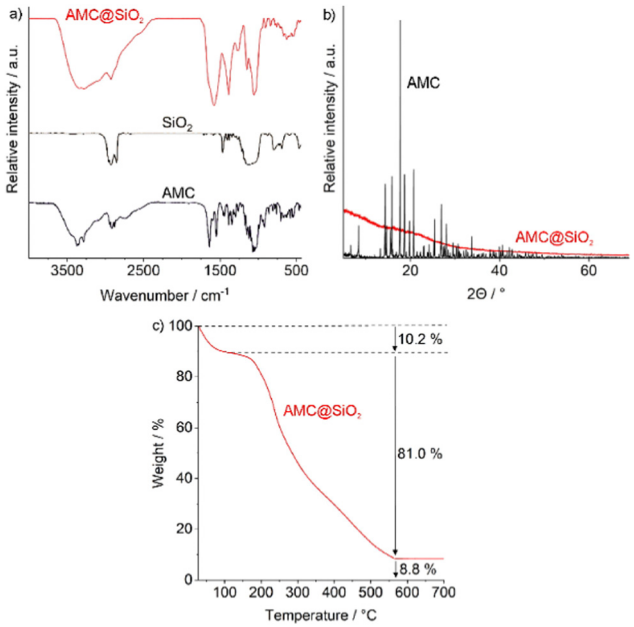


Fig. 4 Chemical composition of the as-prepared AMC@$SiO_2$ core@shell nanocarriers: (a) FT-IR spectrum with pure AMC and $SiO_2$ as references, (b) XRD with AMC as a reference, (c) TG analysis.

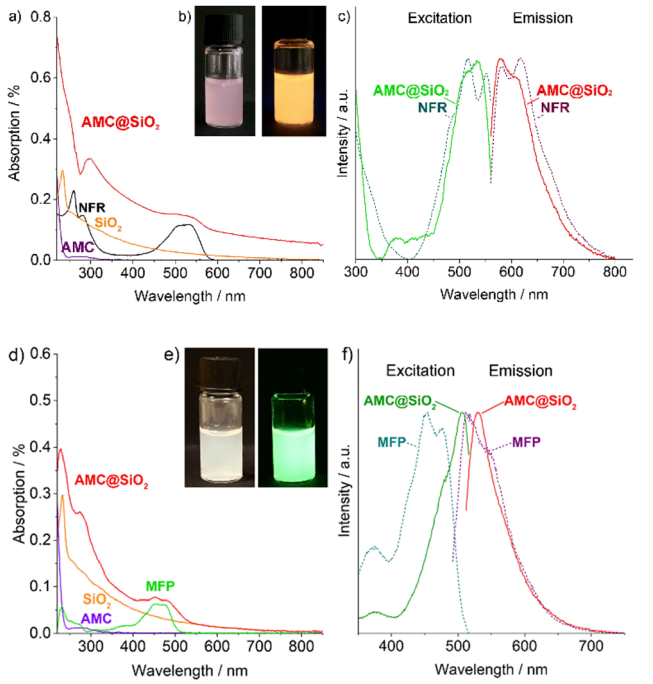


Fig. 5 Optical properties of NFR-labelled (a–c) and MFP-labelled (d–f) AMC@$SiO_2$ core@shell nanocarriers: (a and d) UV-Vis spectrum with AMC@$SiO_2$ (ethanol), $SiO_2$ (ethanol), AMC (in water), and NFR (in water) or MFP (in water) as references, (b and e) photo of suspension in daylight and with excitation (366 nm), (c and f) excitation and emission spectra (recorded with NFR: $\lambda_{em}$ = 575 nm, $\lambda_{exc}$ = 534 nm; MFP: $\lambda_{em}$ = 497 nm, $\lambda_{exc}$ = 531 nm).

can be related to AMC (N : C : H = 1 : 3.8 : 0.6). The residual C/H content (5 wt% C, 0.2 wt% H) can be ascribed to remaining octyl groups. In sum, the as-prepared AMC@$SiO_2$ nanocarriers (after correction for surface-adhered solvents) can be concluded to contain 80 wt% of AMC (0.8 mg $mg^{-1}$), 9 wt% of further organics and water, as well as 11 wt% of $SiO_2$. With this composition, the AMC load of the AMC@$SiO_2$ core@shell nanocarriers is 20- to 100-times higher as reported for polymer- or liposome-based nanocarriers.[6a–d,7] This exceptional drug load also allows to significantly reduce the amount of non-drug by-materials (*e.g.* silica) administered with the nanocarriers, which are non-active but nevertheless may cause toxic effects.

The AMC@$SiO_2$ core@shell nanocarriers can be easily enabled with fluorescence features. Here, for instance, Nuclear Fast Red (NFR) or methylfluorescein phosphate (MFP) were used as orange-light or green-light emitting dyes, added to the aqueous amikacin solution in the synthesis procedure (Fig. 1b). Thereafter, the presence of NFR/MFP can be proven by UV-Vis and photoluminescence spectroscopy (Fig. 5). UV-Vis spectra of NFR-labelled AMC@$SiO_2$ core@shell nanocarriers show the characteristic absorption maxima of NFR (300–350, 450–580 nm) as well as the absorption of $SiO_2$ (<230 nm) (Fig. 5a). The NFR-based absorption is also causative for the reddish appearance of NFR-labelled samples (Fig. 5b). Beside UV-Vis spectra, excitation and emission spectra exhibit the characteristic fluorescence properties of NFR (Fig. 5c). The orange emission of NFR-labelled samples is even visible with the naked eye (Fig. 5b). Similar to NFR, MFP-labelled AMC@$SiO_2$ core@shell nanocarriers show the expected absorption of MFP (400–500 nm) and of $SiO_2$ (<230 nm) (Fig. 5d). Fluorescence spectra indicate the MFP-related excitation (400–550 nm) and emission (500–650 nm) (Fig. 5f). Due to the pH-dependence of the fluorescence of MFP,[19] certain shift of excitation/emission between freely dissolved dye and the MFP-labelled nanocarriers is observed. The green emission of MFP-labelled samples is again even visible with the naked eye (Fig. 5e).

### Antibiotic activity of AMC@$SiO_2$ core@shell nanocarriers

For pulmonal administration of the AMC@$SiO_2$ core@shell nanocarriers (*e.g.* aerosol), their colloidal stability and storage stability are specifically relevant. To this concern, suspensions in water turned out to be less suitable as they show certain agglomeration of the AMC@$SiO_2$ core@shell nanocarriers as well as a continuous AMC release during storage. To this concern, we have redispersed the nanocarriers in DMSO – a solvent, which is even approved for intravenous application[20] and in which AMC is more-or-less insoluble. Dispersing AMC@$SiO_2$ core@shell nanocarriers in DMSO also turned out to be advantageous for storage. Thus, the DMSO suspensions with 5 mg $mL^{-1}$ can be frozen at −30 °C without any change of size or shape of the nanocarriers. Thus, after 10 weeks at −30 °C and warming to room temperature, DLS shows a particle size and particle size distribution similar to the as-prepared DMSO suspensions prior to freezing (Fig. 6a). Taken together, high drug load, high colloidal stability, and good storage stability are very promising for pulmonal application.

Upon addition of the as-prepared DMSO suspensions to water, AMC is continuously released over about 80 min, which

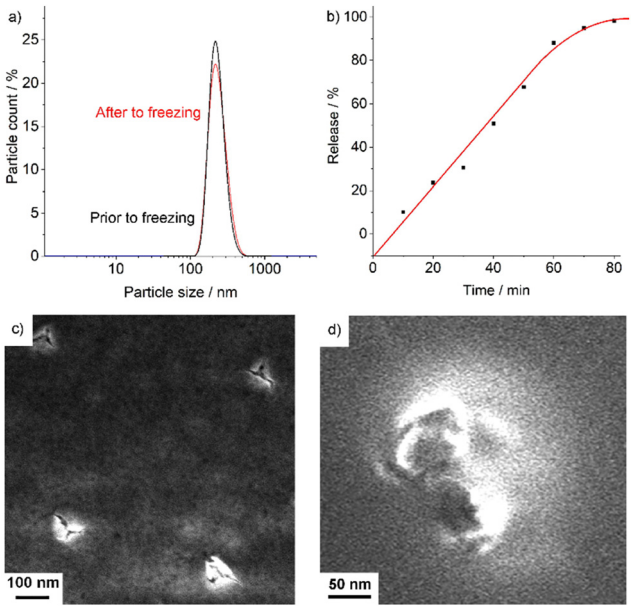


Fig. 6 AMC release of AMC@$SiO_2$ core@shell nanocarriers: (a) particle size according to DLS analysis prior and after freezing in DMSO at −30 °C for 10 weeks, (b) UV-vis spectra showing the AMC release after mixing of DMSO suspensions with water based on the NFR absorption (at 535 nm) in the supernatant after 10–80 min of stirring and separation of the nanocarriers), (c and d) SEM images of nanocarriers after AMC release with considerable cracks in the surface.

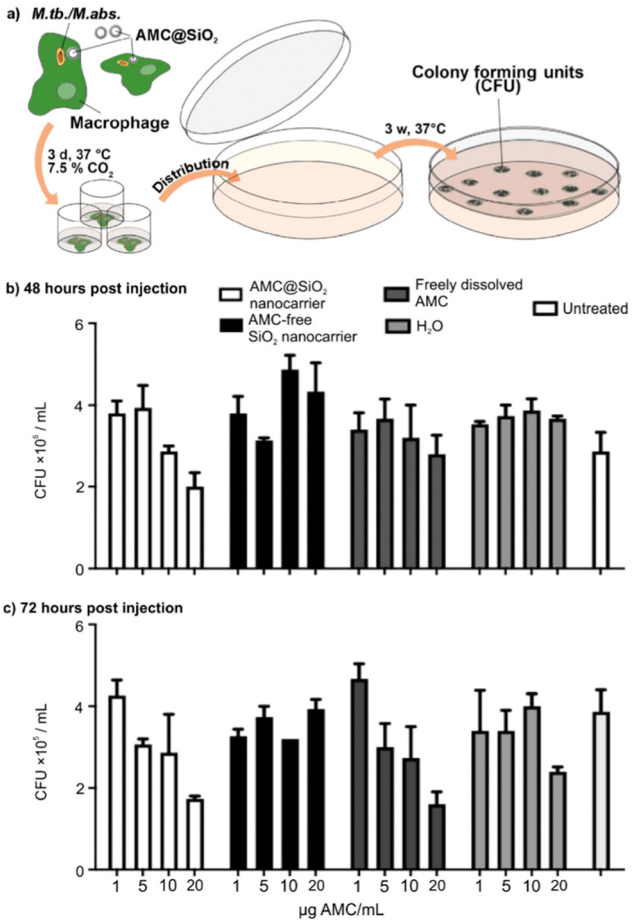


Fig. 7 Antibiotic activity of AMC@$SiO_2$ core@shell nanocarriers against *Mycobacterium tuberculosis*: (a) schema illustrating the incubation procedure and growth of colony forming units (CFU), (b and c) concentration- and time-depending activity against *M.tb.* 48 hours (b) and 72 hours (c) post infection.

can be followed by UV-Vis spectroscopy. Due to the fact that AMC does not exhibit any characteristic absorption in the visible regime, NFR-labelled AMC@$SiO_2$ core@shell nanocarriers were used. In fact, their release can be considered to be largely similar as both AMC and NFR are located in the inner core of the nanocarriers and as both have a similar solubility in water. Accordingly, NFR-labelled AMC@$SiO_2$ core@shell nanocarriers were injected into water and thereafter continuously stirred over periods of 10 to 80 min. Thereafter, the nanocarriers were removed by centrifugation, and the NFR absorption of the supernatant monitored at 535 nm. As a result, a more-or-less linear release of AMC/NFR over about 60 min was observed (Fig. 6b). After 80 min, AMC/NFR was completely released. The solid residue of the remaining nanocarriers was examined by SEM (Fig. 6c and d). The respective images still show $SiO_2$ nanocarriers with considerable cracks in their surface. Thus, it can be assumed that the AMC@$SiO_2$ core@shell nanocarriers break up due to the uptake of water, driven by the high osmotic pressure of the highly polar AMC in the inner nanocarrier core. Thereafter, AMC (and NFR) are released into the solution. Having reached the deep lung (*e.g. via* aerolization), the nanocarriers as well as already released AMC can be taken up by macrophages for transport to the site of the bacteria, whereas silica residues are removed from the lung with the mucus.[21]

As a proof-of-concept study, the anti-mycobacterial activity of the AMC@$SiO_2$ core@shell nanocarriers in comparison to free AMC was examined in murine bone marrow derived macrophages (BMMO) infected *in vitro* with either *M.tb.* (Fig. 7) or *M.abs.* (Fig. 8) for 2 h. Cells were incubated for 0 to 72 h in the presence of either AMC@$SiO_2$ nanocarriers, freely dissolved AMC (both pre-diluted in medium and adjusted to AMC concentrations of 0 to 32 µg $mL^{-1}$, positive control), AMC-free $SiO_2$ nanocarriers or water (negative controls). Cells were lysed, serially diluted, and plated onto 7H11 agar plates to determine the anti-mycobacterial activity by colony-forming-unit (CFU) counts after 3 weeks of incubation at 37 °C (Fig. 7a). AMC@$SiO_2$ suspensions and AMC solutions were employed at identical AMC concentrations.

The CFU data consistently show that neither AMC-free $SiO_2$ nanocarriers nor $H_2O$ affect the growth of *M.tb.* or *M.abs.* in infected BMMO resulting in similar CFU numbers as in untreated cells (Fig. 7b, c and 8b, c). In contrast to AMC-free $SiO_2$ nanocarriers, AMC@$SiO_2$ core@shell nanocarriers show a dose- and time-dependent anti-mycobacterial activity similar to freely dissolved AMC. This finding also confirms a complete release as already indicated in Fig. 6b. Notably, the activity of both free AMC as well as nanocarrier-formulated AMC against *M.tb.* is moderate (Fig. 7b and c). In contrast, both free AMC as well as nanocarrier-formulated AMC show a substantial anti-mycobacterial

 

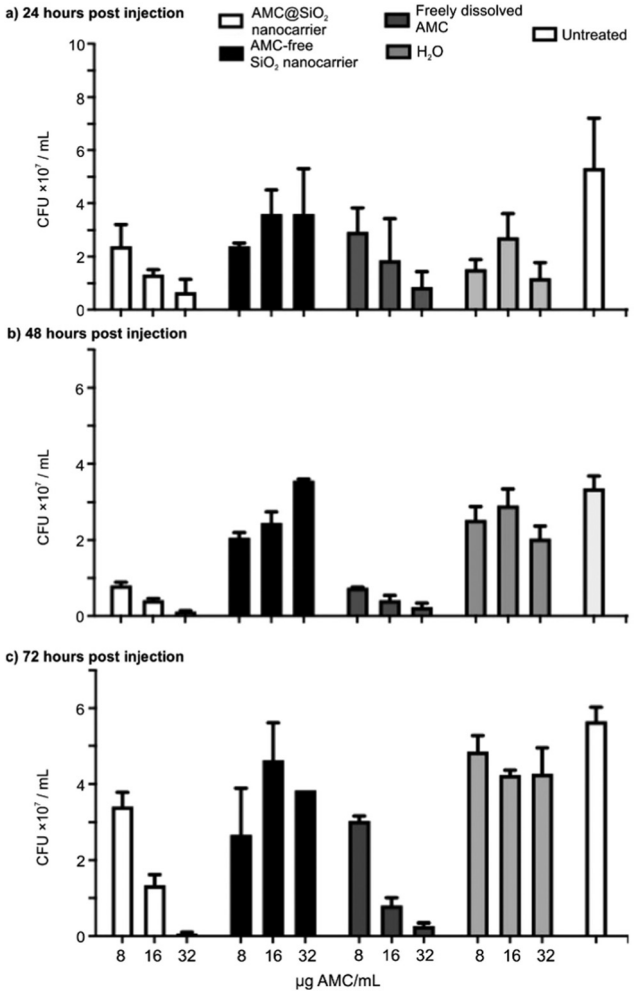


Fig. 8 Antibiotic activity of AMC@$SiO_2$ core@shell nanocarriers against *Mycobacterium abscessus*: (a–c) concentration- and time-depending activity against *M.abs.* 24 hours (a), 48 hours (b), and 72 hours (c) post infection.

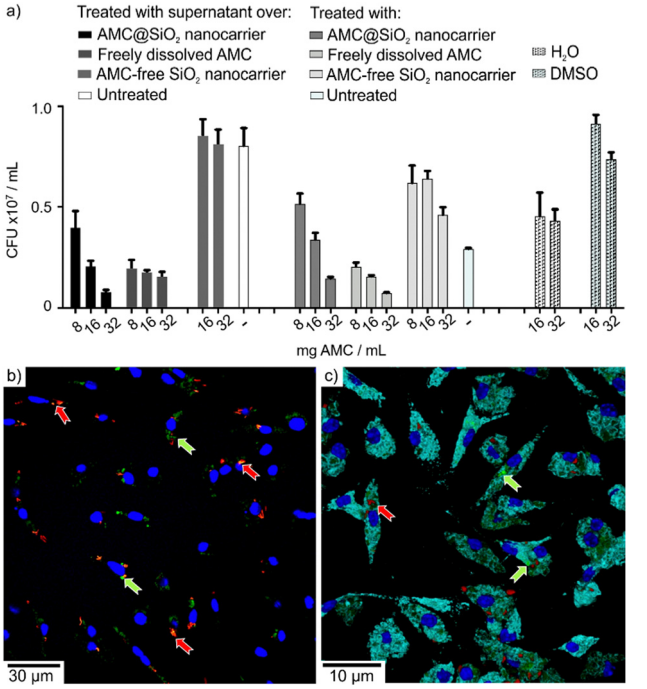


Fig. 9 AMC release and uptake *in vitro*: (a) antibiotic activity of supernatants from AMC@$SiO_2$ core@shell nanocarrier-treated macrophage cultures against *M.abs.* in macrophages with concentration-depending activity against *M.abs.* 48 h post infection of both supernatants retrieved from non-infected macrophage cultures after a 6 h period of incubation with AMC@$SiO_2$ core@shell nanocarriers, AMC-free $SiO_2$ nanocarriers (negative control) or freely dissolved AMC (positive control) in comparison to the directly added compounds; (b and c) confocal laser scanning microscopy of mCherry-expressing *M.abs.* (red; red arrows) infected macrophages treated for 24 h with MFP-labelled AMC@$SiO_2$ core@shell nanocarriers (green; green arrows), stained with DAPI (nuclei, blue) in (b) and with anti-LAMP-1 antibodies (light blue) in (c).

activity against *M.abs.* (Fig. 8b and c). Against *M.abs.*, the AMC@$SiO_2$ core@shell nanocarriers are even slightly more active than freely dissolved AMC over time. Notably, cells treated with AMC@$SiO_2$ core@shell nanocarriers were less affected by the mycobacterial infection compared to untreated ones, indicating both the anti-mycobacterial effect as well as the absence of cytotoxic effects of the $SiO_2$ core@shell nanocarriers system as such.

In order to evaluate the release of the AMC@$SiO_2$ core@shell nanocarriers *in vitro*, culture supernatants from non-infected macrophages were tested, which were incubated for 6 h with AMC@$SiO_2$ core@shell nanocarriers, AMC-free control nanocarriers or freely dissolved AMC (Fig. 9a). The anti-mycobacterial activity of these supernatants was tested on *M.abs.* infected macrophages in comparison to directly added AMC@$SiO_2$ core@shell nanocarriers, AMC-free control nanocarriers or freely dissolved AMC (Fig. 9a). Both, supernatants from macrophage cultures treated with AMC@$SiO_2$ core@shell nanocarriers or free AMC show similar CFUs as directly added AMC@$SiO_2$ core@shell nanocarriers or free AMC, which similar to the results displayed in Fig. 6b indicates a complete release of AMC during the incubation period leading to a similar anti-mycobacterial activity present in the supernatants of treated cells.

Confocal laser scanning microscopy, moreover, reveals the green fluorescence of MFP released together with AMC from MFP-labelled AMC@$SiO_2$ core@shell nanocarriers (Fig. 9b and c), associated with both, *M.abs.* phagosomes as well as LAMP-1 positive compartments, thereby indicating the release of AMC from nanocarriers into intracellular endosomal compartments including mycobacterial phagosomes. The intracellular release of the drug gives rise to the observed biological activity and either points to an efficient membrane crossing ability of the drug itself or an AMC transport *via* endosomal vesicles.

*M.tb.* and *M.abs.* differ in their reproduction time and their capability to grow outside macrophages. Whereas *M.tb.* is a primarily intracellular and slow growing mycobacterium, *M.abs.* is equally capable to grow in- and out-side of macrophages in cell cultures. The result that nanocarriers associated and freely dissolved AMC have a similar efficacy against mycobacteria suggests the release of the drug from the AMC@$SiO_2$ core@shell nanocarriers during interaction with or after the

uptake by the infected BMMO. Such drug release restricted to the site of infection is essential to avoid systemic adverse effects upon *i.v.* therapy. Moreover, AMC@$SiO_2$ core@shell nanocarriers may be applicable by aerosol (including DMSO or lipopilic dispersants) with the additional benefit that it can be directly delivered to the lung as prime target organ similar to the recently clinically approved successful inhalation therapy by nebulized AMC Liposome Inhalation Suspensions (ALIS) to treat ventilator-associated pneumonia and cystic fibrosis (CF) as well as non-CF-associated pulmonary *M.abs*. infections.[22] In difference to ALIS with 4.4% AMC of total nanocarrier mass,[7,22] however, AMC@$SiO_2$ core@shell nanocarriers with 80% AMC of total nanocarrier mass are superior due to a significantly higher drug load.

# Experimental

## Synthesis

**AMC@$SiO_2$ nanocarriers.** 80 mg of amikacin (AMC, $C_{22}H_{43}N_5O_{13}$, 0.14 mmol, Sigma-Aldrich, Germany) were dissolved in 0.7 mL of water and acidified with 0.1 mL HCl (0.1 M). The resulting solution was injected with vigorous stirring into 50 mL of a solution of 50 mL ethanol (absolute, VWR, Germany) with 30 μL of *n*-octyltriethoxysilane (OTES, $CH_3(CH_2)_7Si(OC_2H_5)_3$, 0.01 mmol, Sigma-Aldrich, Germany), 20.0 mg of citric acid ($C_6H_8O_7$, 0.10 mmol, Sigma-Aldrich, Germany), and 1 mg of $NH_4F$ (27 μmol, Sigma-Aldrich, Germany) at 70 °C. After 8 h of continuous stirring and heating, the pH of the suspension was neutralised to about 7 *via* addition of 0.1 mL $NH_3$ solution (0.1 M). Furthermore, a solution of 150 μL tetraethoxysilane (TEOS, $C_8H_{20}O_4Si$, 0.67 mmol, Sigma-Aldrich, Germany) in 5 mL of ethanol were slowly added *via* a syringe pump with a rate of 0.25 mL $h^{-1}$. After additional 2 hours of continuous stirring, 1 mg of $NH_4F$ (27.0 μmol) was added, followed by a second addition of as solution of 150 μL of TEOS (0.67 mmol) in 5 mL of ethanol, again, with a rate of 0.25 mL $h^{-1}$. Again, 1 mg of $NH_4F$ was added and stirring continued for another 24 h to finish of the hydrolysation process. Finally, the resulting suspension was purified three times by centrifugation (10 000 × g, 10 min) and resuspension of the nanoparticles in absolute ethanol to remove salts and excess starting materials. The as-prepared AMC@$SiO_2$ nanocarriers can be stored as a suspension in ethanol or dimethylsulfoxide (DMSO, VWR, Germany) with a concentration of 5 mg $mL^{-1}$.

For fluorescence labelling of the AMC@$SiO_2$ nanocarriers, 3 mg of Nuclear Fast Red (NFR, $C_{14}H_8NNaO_7S$, 8.40 μmol, Sigma-Aldrich, Germany) or 3.9 mg of disodium methylfluorescein phosphate ($Na_2$(MFP), $Na_2C_{21}H_{13}O_8P$, 8.40 μmol, Sigma-Aldrich, Germany) can added to the aforementioned amikacin solution.

**AMC release.** To examine the AMC release out of AMC@$SiO_2$ nanocarriers, 0.3 mL of a suspension of NFR-labelled AMC@$SiO_2$ nanocarriers in DMSO (1 mg $mL^{-1}$ nanocarriers) was injected into a centrifugation tube containing 10 mL of water. After certain period of time (*i.e.*, 10, 20, 30, 40, 50, 60, 70, 80 min), the solid nanocarriers were separated by centrifugation (10 000 × g, 10 min). Thereafter, the absorption of NFR at 535 nm was recorded *via* UV-vis spectroscopy. As AMC does not exhibit any characteristic absorption, AMC cannot be measured directly. Since both AMC and NFR are located in the inner core of the NFR-labelled AMC@$SiO_2$ nanocarriers, their release can be considered to be largely similar.

## Analytical tools

Dynamic light scattering (DLS) was performed to determine the hydrodynamic diameter of the AMC@$SiO_2$ nanocarriers in suspension. To this concern, suspensions in ethanol of DMSO were analysed in polystyrene cuvettes using a Nanosizer ZS (Malvern Instruments, United Kingdom). The same instrument was also used for zeta-potential measurements to examine surface charging and colloidal stability the nanocarriers.

Scanning electron microscopy (SEM) was used to determine the particle size and size distribution, using a Zeiss Supra 40 VP (Zeiss, Germany). Samples were prepared by dappling small droplets of the nanocarrier suspension in ethanol on a silicon wafer, which was left to dry for at least 8 h at room temperature. At least 150 nanoparticles were used to statistically determine the mean particle diameter. The same device was also used for scanning transmission electron microscopy (STEM) to confirm the particle size and examine the inner cavity and shell of the $SiO_2$ nanocarriers.

Transmission electron microscopy (TEM) and high-angle annular dark-field scanning transmission electron microscopy (HAAADF-STEM) were performed with a FEI Osiris microscope (Thermo Fisher Scientific, USA) at 200 kV. TEM samples were prepared by evaporating small droplets of ethanol suspensions on Lacey-film carbon copper TEM grids.

Energy dispersive X-ray spectroscopy (EDXS) was applied to obtain element mappings and to verify the nanocarrier composition. To this concern, a Bruker Quantax system (XFlash detector, Bruker, Germany) was used, which was installed at the FEI Osiris TEM.

Fourier-transform infrared (FT-IR) spectra were recorded with a Bruker Vertex 70 FT-IR spectrometer (Bruker, Germany). For this purpose, 300 mg of dried KBr were mixed with 2 mg of the nanocarriers, pestled, and thereafter pressed into pellets. These pellets were measured in transmission mode in the range of 4000–450 $cm^{-1}$ and baseline corrected.

UV-Vis spectra were recorded on a Shimadzu UV-2700 (Shimadzu, Japan), equipped with a deuterium discharge lamp (180–360 nm) and a quartz halogen lamp (360–800 nm) using an Ulbricht sphere. Samples were deposited in quartz glass cuvettes by diluting the as-prepared suspensions with ethanol to 25.0 μg $mL^{-1}$. Solutions of the dye in ethanol were used as references at concentrations of 0.25 μg $mL^{-1}$. Spectra of the pure solvent were recorded in addition and used for baseline correction.

Differential thermal analysis/thermogravimetry (DTA/TG) was measured using a STA409C device (Netzsch, Germany). The AMC@$SiO_2$ nanocarriers were predried, and samples of 15 mg were heated to 1200 °C with a heating rate of 5 K $min^{-1}$.

 

Elemental analysis (EA) (C/H/N/S analysis) of predried nanocarriers was performed *via* thermal combustion with an Elementar Vario Microcube device (Elementar, Germany) at a temperature of about 1100 °C.

*In vitro* efficacy studies in mycobacteria-infected macrophages. To assess the anti-mycobacterial activity of AMC@$SiO_2$ nanocarriers compared to free AMC, murine bone marrow derived macrophages (BMMO, mouse strain C57BL/6 J) were generated as described. BMMO were seeded at $1 \times 10^5$ cells per well in culture medium (DMEM/10% FBS/100 μg L-glutamine/10% L929 culture supernatant) for 24 h and subsequently incubated with *M.tb.* strain H37Rv or *M.abs.* at a Multiplicity Of Infection (MOI) of 3 at 37 °C/7.5% $CO_2$ for 2 h. To remove the extracellular mycobacteria, cultures were washed with DMEM, and AMC@$SiO_2$ nanocarrier suspensions (in DMSO) or freely dissolved AMC (in water) was added at the concentration indicated. Upon different incubation-time periods as indicated, cells were serially diluted in water/0.5% BSA/0.1%Tween 80, plated onto 7H11 agar plates, and incubated at 37 °C for 4 weeks before the colony forming units (CFU) were counted. AMC-free $SiO_2$ nanocarriers (in DMSO), freely dissolved AMC (in water), and pure water served as negative and positive controls, respectively. Additional controls included supernatants from non-infected macrophage cultures treated with AMC@$SiO_2$ nanocarriers, AMC-free $SiO_2$ nanocarriers, and freely dissolved AMC retrieved after a 6 h incubation period and centrifugation at 10 000 rpm to remove the nanocarrier remains.

## Conclusions

AMC@$SiO_2$ core@shell nanocarriers (AMC: amikacin) with an outstanding AMC load of 80% of the total nanocarrier mass were prepared *via* a solvent–antisolvent approach. Such nanocarriers are shown for the first time and outperform current AMC-containing nanocarriers by a 20- to 100-times higher drug load. With 80% drug load, AMC@$SiO_2$ core@shell nanocarriers exhibit an exceptionally high drug load for silica nanoparticles, in general. The nanocarrier structure exhibits an inner AMC core with about 200 nm in size, which is encapsulated by a silica shell with a thickness of about 20 nm. The silica shell protects the drug core and supports the dispersibility of the nanocarriers. In accordance with the high drug load, moreover, the amount of non-active but potentially toxic by-materials is significantly reduced. For storage and administration of the nanocarriers, DMSO turned out to be a suitable solvent and contained the nanocarriers with 5 mg $mL^{-1}$. Moreover, frozen DMSO suspensions are ideal for long-term storage and do not show any change of size and shape. Based on fluorescence-labelled nanocarriers, the AMC release was shown to be complete after about 80 min. Such fast and complete drug release is also a difference and potential advantage to many state-of-the-art $SiO_2$-based nanocarriers, which show slow and often incomplete drug release.

As a proof-of-the-concept, the activity of AMC@$SiO_2$ core@shell nanocarriers was evaluated in bone marrow derived macrophages (BMMO) that were infected with *Mycobacterium tuberculosis* (*M.tb.*) or *Mycobacterium abscessus* (*M.abs.*). Both highly relevant bacterial pathogens are notoriously associated with multidrug-resistance. The AMC-nanocarrier formulations show similar activities as freely dissolved AMC against *M.abs* and *M.tb.*, with especially promising results in the case of *M.abs.* In sum, the novel synthesis approach and materials concept with the outstanding drug load (0.8 mg $mg^{-1}$) of a polar, water-soluble drug in a thin silica shell can be transferred to other drugs to treat further types of bacteria and mycobacteria. Based on the high drug load, high colloidal stability and good storage stability, finally, aerosol-based administration seems most promising when aiming at pulmonal infections.

## Author contributions

MR performed the nanocarrier synthesis and characterization in the group of CF. He also prepared a draft manuscript. *In vitro* studies were performed by NR in the group of UES. CF and UES supervised the studies and prepared the manuscript.

## Conflicts of interest

There are no conflicts to declare.

## Acknowledgements

The authors acknowledge funding by VDE/VDI through the German Federal Ministry of Education and Research (BMBF) within the collaborative research project ANTI-TB. MR and CF acknowledge the Deutsche Forschungsgemeinschaft (DFG) for funding within the project Research Training Group 2039 ''Molecular architecture for fluorescent cell imaging''. Big thanks go out to Laurent Cremer, Université de Montpellier, France, for providing us with a *M. abscessus* strain expressing mCherry. Finally, NR and UES specifically acknowledge Kristine Hagens for her expert technical assistance in the anti-mycobacterial efficacy experiments.

## Notes and references

1 (*a*) A. Maxwell, V. Ghate, J. Aranjani and S. Lewis, *Life Sci.*, 2021, **284**, 119883; (*b*) M. S. Ramirez and M. E. Tolmasky, *Molecules*, 2017, **22**, 2267.
2 N. Ahmad, S. D. Ahuja, O. W. Akkerman, J.-W. C. Alffenaar, L. F. Anderson, P. Baghaei, D. Bang, P. M. Barry, M. L. Bastos and D. Behera, *et al.*, *Lancet*, 2018, **392**, 821–834.
3 M. Bassetti, A. Vena, A. Russo and M. Peghin, *Drugs*, 2020, **80**, 1309–1318.
4 (*a*) M. Izci, C. Maksoudian, B. B. Manshian and S. J. Soenen, *Chem. Rev.*, 2021, **121**, 1746–1803; (*b*) M. Bjornmalm,

K. J. Thurecht, M. Michael, A. M. Scott and F. Caruso, *ACS Nano*, 2017, **11**, 9594–9613.

5 M. Klinger-Strobel, C. Lautenschläger, D. Fischer, J. G. Mainz, T. Bruns, L. Tuchscherr, M. W. Pletz and O. Makarewicz, *Expert Opin. Drug Delivery*, 2015, **12**, 1351–1374.

6 (*a*) S. Abdelghany, T. Parumasivam, A. Pang, B. Roediger, P. Tang, K. Jahn, W. J. Britton and H.-K. Chan, *J. Drug Delivery Sci. Technol.*, 2019, **52**, 642–651; (*b*) S. Fatima, A. K. Panda, S. Talegaonkar, Z. Iqbal and F. J. Ahmad, *J. Pharm. BioAllied Sci.*, 2019, **11**, 83–95; (*c*) S. Fatima, Z. Iqbal, A. K. Panda, M. Samim, S. Talegaonkar and F. J. Ahmad, *Colloids Surf., B*, 2018, **169**, 206–213; (*d*) P. Sabaeifard, A. Abdi-Ali, C. Gamazo, J. M. Irache and M. R. Soudi, *J. Med. Microbiol.*, 2017, **66**, 137–148; (*e*) P. Sabaeifard, A. Abdi-Ali, M. R. Soudi, C. Gamazo and J. M. Irache, *Eur. J. Pharm. Sci.*, 2016, **93**, 392–398; (*f*) Y. Zhang, J. M. Pelet, D. A. Heller, Y. Dong, D. Chen, Z. Gu, B. J. Joseph, J. Wallas and D. G. Anderson, *Adv. Mater.*, 2013, **25**, 4641–4645.

7 J. Zhang, F. Leifer, S. Rose, D. Y. Chun, J. Thaisz, T. Herr, M. Nashed, J. Joseph, W. R. Perkins and K. DiPetrillo, *Front. Microbiol.*, 2018, **16**, 915.

8 (*a*) M. Alizadeh, M. Amiri and A. Bezaatpour, *Curr. Drug Delivery*, 2021, **18**, 761–769; (*b*) G. D. Saratale, R. G. Saratale, G. S. Ghodake, S. Shinde, D.-Y. Kim, A. A. Alyousef, M. Arshad, A. Syed, D. Pant and H.-S. Shin, *Nanomater*, 2020, **10**, 997; (*c*) A. Kaur and R. Kumar, *RSC Adv.*, 2019, **9**, 1095–1105; (*d*) T. Zheng, Y. Y. L. Sip, M. B. Leong and Q. Huo, *Colloids Surf., B*, 2018, **164**, 185–191.

9 H. Ayazi, O. Akhavan, M. Raoufi, R. Varshochian, M. N. S. Hosseini and F. Atyabi, *Colloids Surf., B*, 2020, **186**, 110712.

10 (*a*) M. Vallet-Regí, F. Schüth, D. Lozano, M. Colilla and M. Manzano, *Chem. Soc. Rev.*, 2022, **51**, 5365–5451; (*b*) M. Manzano and M. Vallet-Regi, *Adv. Funct. Mater.*, 2020, **30**, 1902634; (*c*) W. Q. Lim, S. Z. F. Phua, H. V. Xu, S. Sreejith and Y. Zhao, *Nanoscale*, 2016, **8**, 12510–12519.

11 (*a*) C. W. Ang, L. Tan, Z. Qu, N. P. West, M. A. Cooper, A. Popat and M. A. T. Blaskovich, *ACS Biomater. Sci. Eng.*, 2022, **8**, 4196–4206; (*b*) J. O. Tella, J. A. Adekoya and K. O. Ajanaku, *R. Soc. Open Sci.*, 2022, **9**, 220013; (*c*) B. Beitzinger, F. Gerbl, T. Vomhof, R. Schmid, R. Noschka, A. Rodriguez, S. Wiese, G. Weidinger, L. Ständker, P. Walther, J. Michaelis, M. Liden and S. Stenger, *Adv. Healthcare Mater.*, 2021, **10**, 100453.

12 (*a*) M. D. Johansen, J.-L. Herrmann and L. Kremer, *Nat. Rev. Microbiol.*, 2020, **18**, 392–407; (*b*) M.-R. Lee, C.-J. Tsai, J.-Y. Hu, S.-W. Lee, J.-C. Ko, H.-C. Wang, C.-J. Yu, L.-N. Lee and P.-R. Hsueh, *Future Microbiol.*, 2016, **11**, 491–500.

13 (*a*) Y. Yu, J. Chen, S. Liu and D. Cheng, *J. Mater. Chem. B*, 2021, **9**, 6044–6055; (*b*) D. K. Yi, S. T. Selvan, S. S. Lee, G. C. Papaefthymiou, D. Kundaliya and J. Y. Darshan, *J. Am. Chem. Soc.*, 2005, **127**, 4990–4991.

14 S. Wolf and C. Feldmann, *Angew. Chem., Int. Ed.*, 2016, **55**, 15728–15752.

15 (*a*) R. Jog and D. J. Burgess, *J. Pharm. Sci.*, 2017, **106**, 39–65; (*b*) A. A. Thorat and S. V. Dalvi, *Chem. Eng. J.*, 2012, **181–182**, 1–34.

16 V. K. LaMer and R. H. J. Dinegar, *J. Am. Chem. Soc.*, 1950, **72**, 4847–4854.

17 Y. Han, Z. Lu, Z. Teng, J. Liang, Z. Guo, D. Wang, M.-Y. Han and W. Yang, *Langmuir*, 2017, **33**(23), 5879–5890.

18 A. R. West, *Solid State Chemistry and Its Applications*, Wiley, Chichester, 2nd edn, 2022.

19 N. O. Mchedlov-Petrossyan, T. A. Cheipesh, S. V. Shekhovtsov, A. N. Redko, V. I. Rybachenko, I. V. Omelchenko and O. V. Shishkin, *Spectrochim. Acta, Part A*, 2015, **150**, 151–161.

20 M. Colucci, F. Maione, M. C. Bonito, A. Piscopo, A. di Giannuario and S. Pieretti, *Pharmacol. Res.*, 2008, **57**, 419–425.

21 (*a*) R. A. Fisher, B. Gollan and S. Helaine, *Nat. Rev. Microbiol.*, 2017, **15**, 453–464; (*b*) J. G. Chan, J. Wong, Q. T. Zhou, S. S. Leung and H. K. Chan, *AAPS Pharm. Sci. Tech.*, 2014, **15**, 882–897.

22 (*a*) S. M. H. Zweijpfenning, R. Chiron, S. Essink, J. Schildkraut, O. W. Akkerman, S. Aliberti, J. Altenburg, B. Arets, E. van Braeckel and B. Delaere, *et al.*, *Chest*, 2022, **162**, 76–81; (*b*) E. Tavernier, F. Barbier, F. Meziani, J.-P. Quenot, J.-E. Herbrecht, M. Landais, D. Roux, P. Seguin, D. Schnell and A. Veinstein, *et al.*, *BMJ Open*, 2021, **11**, e048591.

 